REFERENCES

1. Padaeng Industry Public (online). Available from: www.padaeng.co.th. [10.12.2004]
2. M. Pelino. Recycling of jarosite waste in the production of glass and glass ceramic materials. Interceram 47 (1998): 22-26.
3. M. Pelino. Recycling of zinc hydrometallurgical wastes in glass and glass ceramic materials. Waste Management 20 (2000): 561-568.
4. P. Pisciella, S. Crisucci, A. Karamanov, M. Pelino. Chemical durability of glasses obtained by vitrification of industrial wastes. Waste Management 21 (2001): 1-9.
5. Mazimina Romero and Jesus Ma. Rincon. Surface and bulk crystallization of glass-ceramic in the Na_2O-CaO-ZnO-PbO-Fe_2O_3-Al_2O_3-SiO_2 system derived from a goethite waste. Journal of the American Ceramic Society 82 (1999): 1313-1317.
6. W. Vogel. Chemistry of glass. The United States of America: The American Ceramic Society, 1985.
7. Wolfram Holand and George Beall. Glass-ceramic technology. The United States of America: The American Ceramic Society, 2002.
8. D. G Holloway. The physical properties of glass. Great Britain: Taylor & Francis, 1973.
9. W. D. Kingery, H. K. Bowen, D.R. Uhlmann. Introduction to ceramics. Singapore: John Wiley & Sons (SEA) Pte. Ltd., 1991.
10. Arun K. Varshneya. Fundamentals of inorganic glasses. The United States of America: Acedemic Press, 1994.
11. Robert H. Doremus. Glass science 2nd edition. The United States of America: John Wiley & Sons, 1994.
12. Padaeng Industry Public Co. Ltd. The brochure of zinc in everyday life
13. Alexander Karamanov and Mario Pelino. Evaluation of degree of crystallization in glass-ceramics by density measurements. Journal of the European Ceramic Society 19 (1999): 649-654.

14. Alexander Karamanov, Carlo Cantalini, Mario Pelino and Alessandro Hreglich. Kinetics of phase formation in Jarosite glass-ceramic. Journal of the European Ceramic Society 19 (1999): 527-533.

15. M. Romero and J. Ma. Rincon. Preparation and properties characterization of high iron content glasses obtained by recycling goethite industrial waste. Journal of the European Ceramic Society 18 (1998): 153-160.

16. M. Pelino, C. Cantalini, and J. Ma. Rincon. X-ray microanalysis of crucible-glass interphases on melting of glasses obtained from goethite waste. Journal of Materials Science 32 (1996): 4655-4660.

17. Alexander Karamanov, Mario Pelino and Alessandro Hreglich. Sintered glass-ceramics from municipal solid waste-incinerator fly ashes-part I: the influence of the heating rate of the heating rate on the sinter-crystallization. Journal of the European Ceramic Society 23 (2003): 827-832.

18. Alexander Karamanov, Mario Pelino, Milena Salvo and Ilidko Metekovits. Sintered glass-ceramics from incinerator fly ashes. Part II. The influence of the particle size and heat-treatment on the properties. Journal of the European Ceramic Society 23 (2003): 1609-1615.

19. Luisa Barbieri, Anna Maria Ferrari, Isabella Lancellotti and Chistina Leonelli. Crystallization of (Na_2O-MgO)-CaO-Al_2O_3-SiO_2 glassy systems formulated from waste proeducts. Journal of the American Ceramic Society 83 (2000): 2515-2520.

20. Young Jun Park and Jong Heo. Conversion to glass-ceramics from glasses made by MSW incinerator fly ash for recycling. Ceramics International 28 (2002): 689-694.

21. T.W. Cheng, T.H. Ueng, Y.S. Chen and J.P Chiu. Production of glass-ceramic from incinerator fly ash. Ceramics International 28 (2002): 779-783.

22. Luisa Barbieri, Isabella Lancellotti, Tiziano Manfredini and Gian Carlo Pellacani. Nucleation and crystallization of new glasses from fly ash originating from thermal power plants. Journal of the American Ceramic Society 84 (2001): 1851-1858.

23. Luisa Barbieri, Anna Corradi and Isabella Lancellotti. Bulk and sintered glass-ceramics by recycling municipal incinerator bottom ash. Journal of the European Ceramic Society 20 (2000): 1637-1643

24. M. Romero, J. Ma. Rincon, A. Acosta. Effect of iron oxide content on the crystallization of a diopside glass-ceramic glaze. Journal of the European Ceramic Society 22 (2002): 883-890.

25. G.F. Piepel. Mixsoft-software for the design and analysis of mixture and other constrained region experiments. User's guide version 2.31. The United States of America, 2000.

26. Method 1311 Toxic characteristic leaching procedure (online). Available from: http://www.epa.gov/epaoswer/hazwaste/test/pdfs/1311. July, 1992.

27. E. Shelby. Introduction to Glass science and Technology. New York: The Royal Society of Chemistry, 1997.

28. Young Jun Park and Jong Heo. Conversion to glass-ceramics from glasses made by MSW incinerator fly ash for recycling. Ceramics International 28 (2002): 689-694.

29. Michel W. Barsoum. Fundametal of ceramics. Singapore: MacGraw-Hill Companies, 1997.

APPENDICES

APPENDIX A

The suitable percent of oxides in each glass follow Table 3.2 was calculated by Z + 30% waste. Where, Z is the percent of added-oxides from other sources. Silica sand, boric acid ($B_2O_3 \cdot 3H_2O$), soda ash (Na_2CO_3), limestone ($CaCO_3$), magnesium carbonate ($MgCO_3$), zinc oxide, alumina and iron oxide were used as a source of SiO_2, B_2O_3, Na_2O, CaO, MgO, ZnO, Al_2O_3 and Fe_2O_3, respectively.

Calculation of added-oxide percent from other sources is given as an example by a glass system of GC#1 as shown in Table A-1. Firstly oxide percent of GC#1 (A) from Table 3.2 and oxide percent of 30% waste (B) from Table 3.3, have been considered. Percent of added-oxides (Z) derived from the deduction of A from B.

Table A-1 Calculation percent of added-oxides (%wt)

Oxides	GC#1 (A)	30% waste (B)	% added-oxide (Z) (Z = A-B)
SiO_2	45.00	6.80	38.20
B_2O_3	15.00	0.00	15.00
Na_2O	15.00	0.19	14.81
CaO	20.00	4.93	15.07
MgO	0.00	0.09	0.00
ZnO	1.00	0.93	0.07
Al_2O_3	1.00	1.10	0.00
Fe_2O_3	3.00	2.20	0.80

The percent of each added-oxide (Z) was then used as a basic factor for further calculation of their raw material sources (W) as described in Table A-2 which is based on eq. A-1 as follow:

$$W = \frac{(Z \times X)}{Y} \qquad \text{(eq. A-1)}$$

Where, W is percent of oxide resources used as raw material

Z is percent of added-oxide

X is molecular weight of oxide compounds

Y is molecular weight of oxide

e.g. Calculation of percent of boric acid ($B_2O_3 \cdot 3H_2O$) used as a source of added-B_2O_3 (W) in GC#1

$$W = \frac{(15 \times 124)}{70} = 26.57$$

Where, W is percent of boric acid used as a source of added-B_2O_3 = 26.57

Z is percent of added-B_2O_3 = 15.00

X is molecular weight of $B_2O_3 \cdot 3H_2O$ = 124

Y is molecular weight of B_2O_3 = 70

This equation was applied for all eight major oxides in each glass system to calculate percent of raw materials used as sources of added-oxides. Percent of eight raw materials used as sources of added-oxides were calculated for twenty-five glass systems as shown in Table 3.4. These portions of raw materials were then mixed with 30% of zinc waste ready for preparation of glasses.

Table A-2 calculation of raw materials used for GC#1 glass system

(Z) / (W)	SiO_2	B_2O_3	Na_2O	CaO	MgO	ZnO	Al_2O_3	Fe_2O_3
	38.20	15.00	14.81	15.07	0.00	0.07	0.00	0.80
Silica sand (SiO_2) X = SiO_2 = 60 (Y)	38.20							
Boric acid ($B_2O_3 \cdot 3H_2O$) MW = B_2O_3+3(H_2O) X =[70(Y)+54] = 124		26.57						
Soda ash (Na_2CO_3) MW = Na_2O+CO_2 X = [62(Y)+44] = 106			25.32					
Limestone ($CaCO_3$) MW = CaO+CO_2 X = [56(Y)+44] = 100				26.91				
Magnesium carbonate ($MgCO_3$) MW = MgO + CO_2 X = [40(Y)+44] = 84					0.00			
Zinc oxide (ZnO) X = ZnO = 81(Y)						0.07		
Alumina (Al_2O_3) X = Al_2O_3 = 102(Y)							0.00	
Iron oxide (Fe_2O_3) X = Fe_2O_3 = 160(Y)								0.80

APPENDIX B

Fig. B-1 Images of melted glasses

G#1	G#3	G#4	G#5	G#6
				
G#8	G#9	G#10	G#11	G#12
				
G#14	G#16	G#17	G#18	G#19
				
G#20	G#21	G#22	G#23	G#24
				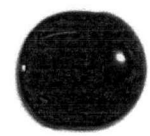
G#2	G#5	G#13	G#15	G#25
				

APPENDIX C

Table C-1 Percent volume shrinkage of glass-ceramics

	Heat-treatment conditions			
GC#	A	B	C	D
2	12.99	35.96	35.41	31.76
3	16.24	32.88	31.67	29.96
4	15.33	32.10	32.61	29.77
5	3.29	34.99	33.69	30.03
6	13.68	33.06	31.21	29.15
7	12.73	34.02	32.00	28.96
8	11.59	35.28	31.28	28.71
10	1.68	35.08	34.70	32.17
18	6.18	33.39	32.83	29.97
19	11.36	34.89	31.68	28.59
24	9.17	34.22	34.19	27.83
22	24.24	34.93	32.69	27.01
23	21.73	33.11	27.72	21.26
1	19.35	28.88	0.13	-1.00
9	30.68	30.61	23.04	24.26
11	13.54	30.18	26.03	16.68
12	2.46	32.05	31.38	22.25
20	18.81	30.56	24.73	24.63
16	10.45	31.11	31.04	28.92
13	2.51	27.75	33.90	31.52
14	2.27	24.62	33.52	31.23
15	1.42	12.93	32.84	33.09
17	2.44	22.84	27.22	35.78
21	1.70	29.57	32.11	28.98
25	1.93	17.53	23.39	33.41

Table C-2 Bulk density of glass-ceramics

	Heat-treatment conditions			
G#	A	B	C	D
2	1.98	2.68	2.69	2.57
3	2.03	2.55	2.53	2.48
4	2.04	2.56	2.65	2.58
5	1.88	2.74	2.71	2.57
6	2.03	2.62	2.55	2.52
7	1.97	2.56	2.48	2.39
8	1.89	2.55	2.46	2.42
10	1.75	2.68	2.67	2.57
18	1.82	2.57	2.56	2.46
19	1.86	2.53	2.44	2.36
24	1.91	2.67	2.45	2.43
22	2.27	2.65	2.63	2.54
23	2.24	2.64	2.46	2.42
1	2.18	2.52	1.80	1.78
9	2.45	2.45	2.24	2.29
11	2.09	2.59	2.43	2.18
12	1.79	2.63	2.56	2.40
20	2.03	2.38	2.24	2.25
16	1.86	2.43	2.40	2.35
13	1.73	2.33	2.56	2.50
14	1.74	2.28	2.56	2.50
15	1.67	1.91	2.46	2.47
17	1.71	2.21	2.35	2.68
21	1.76	2.46	2.58	2.75
25	1.71	2.06	2.23	2.62

Table C-3 Percent water absorption of glass-ceramics

	Heat-treatment conditions			
GC#	A	B	C	D
2	13.31	0.07	0.04	0.03
3	11.75	0.10	0.11	0.20
4	12.08	0.08	0.19	0.26
5	17.16	0.07	0.10	0.09
6	12.57	0.04	0.05	0.05
7	12.71	0.05	0.03	0.07
8	14.73	0.01	0.04	0.07
10	20.46	0.10	0.02	0.09
18	17.78	0.06	0.16	0.12
19	15.16	0.08	0.09	0.24
24	15.81	0.08	0.11	0.27
22	6.94	0.15	0.04	0.24
23	8.04	0.17	0.03	0.04
1	9.51	0.16	0.12	0.23
9	3.13	0.17	0.07	0.11
11	11.86	0.17	0.10	0.28
12	19.04	0.16	0.06	0.15
20	10.81	0.08	0.07	0.04
16	14.89	0.08	0.09	0.10
13	19.10	4.12	0.03	0.20
14	18.57	4.95	0.03	0.14
15	20.60	13.09	0.19	0.11
17	21.59	8.00	6.91	0.28
21	20.51	4.74	4.11	0.12
25	20.48	11.28	9.12	0.00

Table C-4 Percent apparent porosity of glass-ceramics

	Heat-treatment conditions			
GC#	A	B	C	D
2	26.41	0.19	0.10	0.07
3	23.93	0.26	0.28	0.49
4	24.74	0.21	0.51	0.67
5	32.39	0.18	0.27	0.24
6	25.59	0.11	0.14	0.13
7	25.08	0.13	0.07	0.18
8	27.87	0.03	0.09	0.18
10	35.91	0.26	0.04	0.23
18	32.40	0.15	0.42	0.29
19	28.31	0.20	0.21	0.57
24	30.39	0.20	0.26	0.11
22	15.80	0.39	0.11	-0.01
23	18.09	0.45	0.07	0.54
1	20.80	0.39	0.21	0.41
9	7.69	0.42	0.16	0.26
11	24.87	0.43	0.24	0.61
12	34.28	0.43	0.16	0.37
20	22.04	0.19	0.15	0.10
16	27.79	0.19	0.22	0.23
13	33.18	9.63	0.07	0.50
14	32.49	11.34	0.07	0.34
15	34.57	25.07	0.47	0.26
17	36.97	17.73	16.31	0.76
21	36.16	11.72	10.65	0.76
25	35.21	23.33	20.38	1.07

APPENDIX D

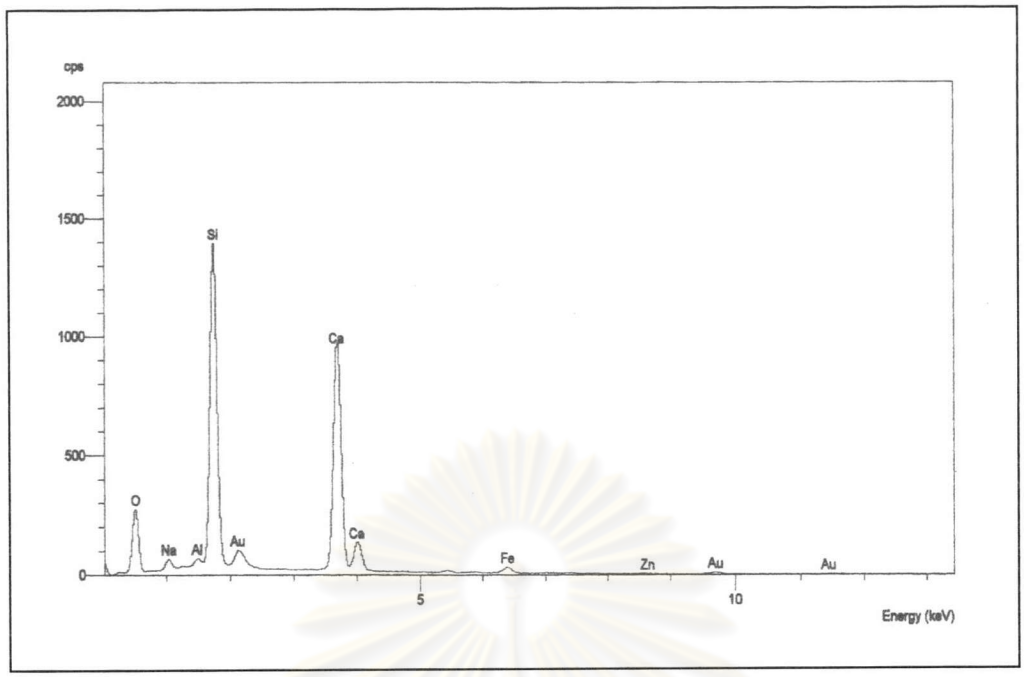

Fig.D-1 EDS spectra of acicular crystal area (A) in GC#24 heat-treated at condition C

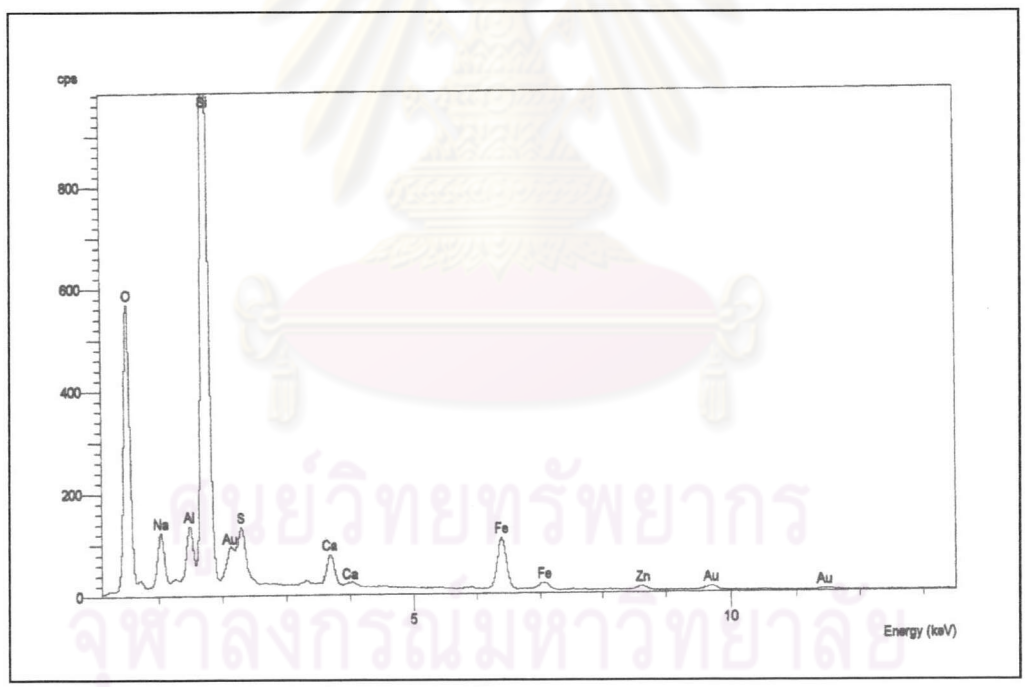

Fig.D-2 EDS spectra of glassy matrix (B) in GC#24 heat-treated at condition C

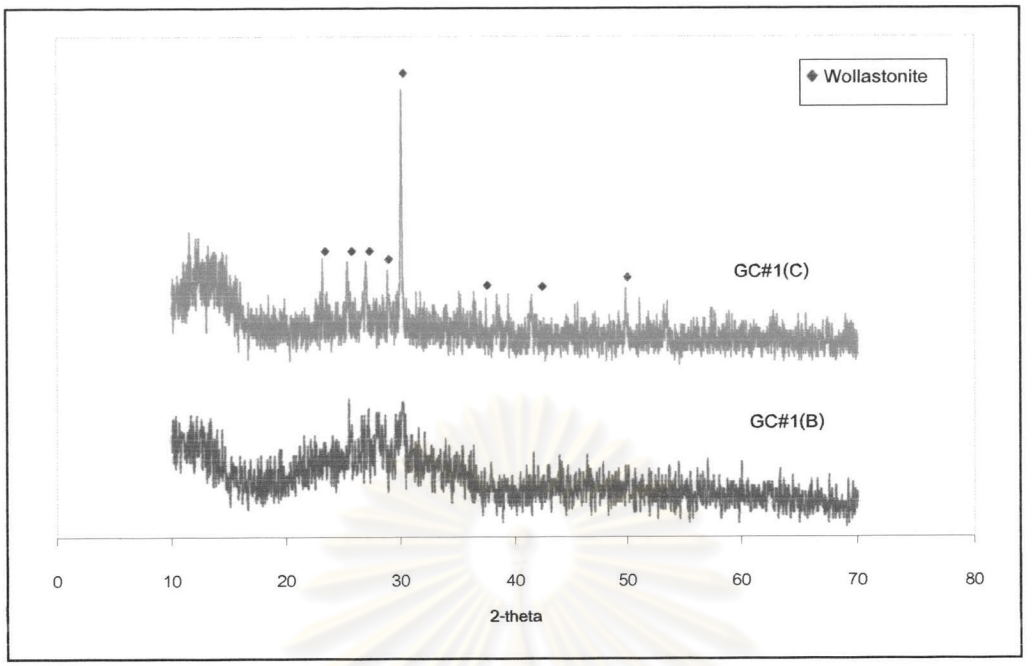

Fig.D-3 XRD patterns of GC#1 heat-treated at condition B and C

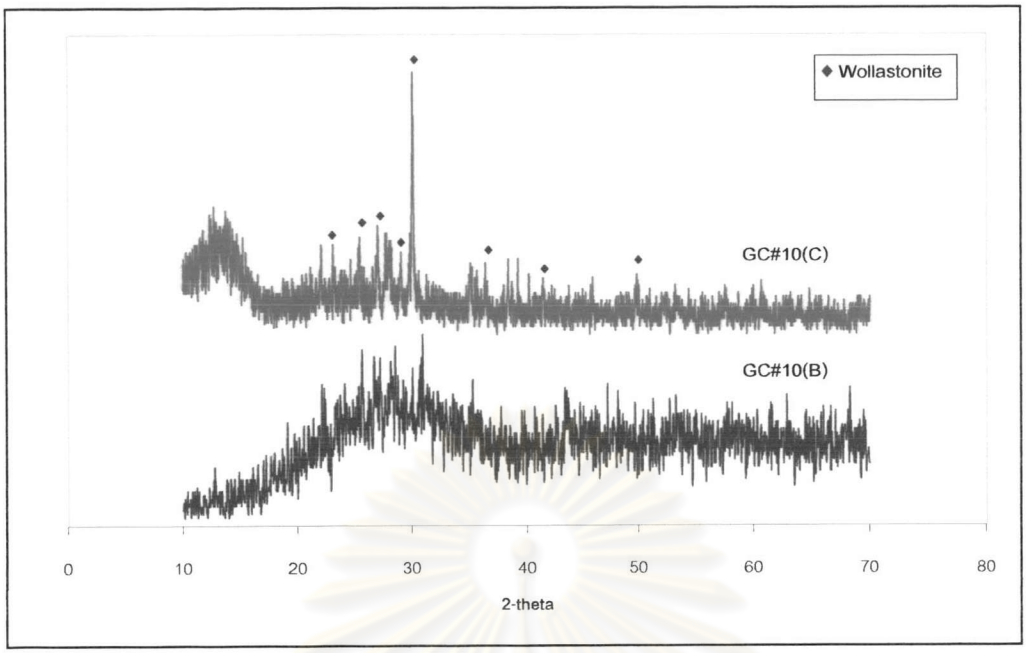

Fig.D-4 XRD patterns of GC#10 heat-treated at condition B and C

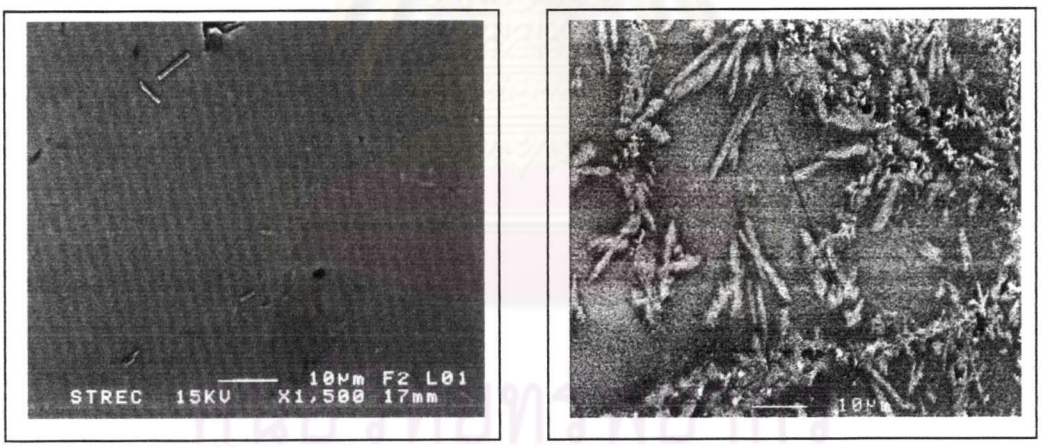

(a) (b)

Fig.D-5 SEM micrographs (1500x) of wollastonite-ferroan phase observed in GC#10 after heat-treatment at condition B (a) C (b)

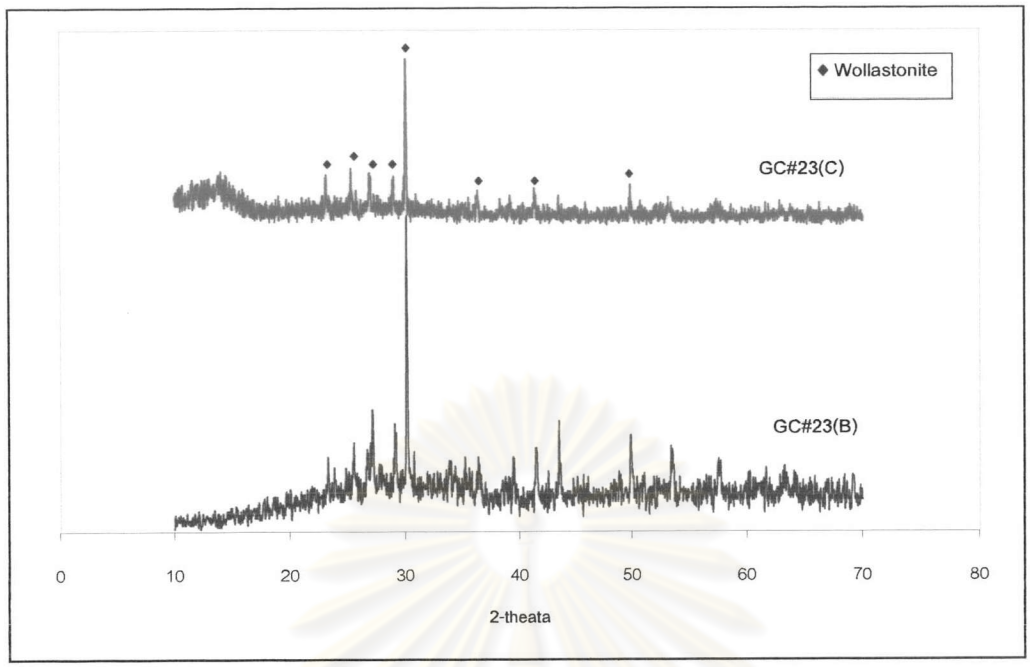

Fig.D-6 XRD patterns of GC#23 heat-treated at condition B and C

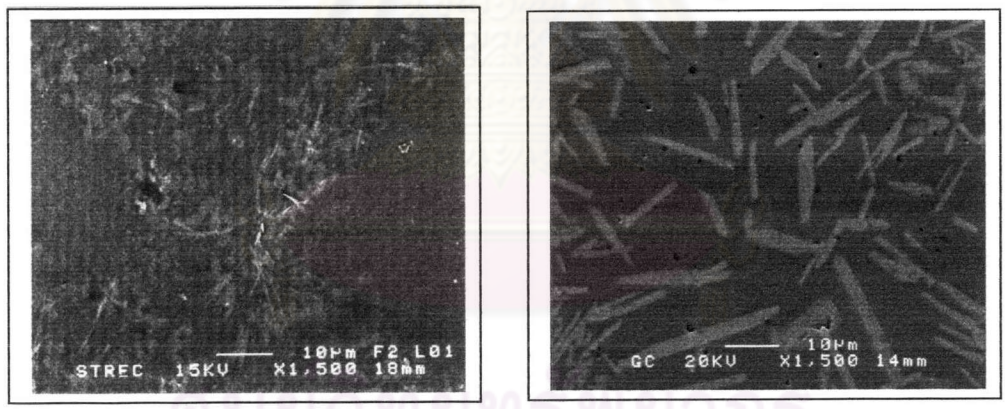

(a) (b)

Fig. D-7 SEM micrographs (1500x) of wollastonite-ferroan phase observed in GC#23 after heat-treatment at condition B (a) C (b)

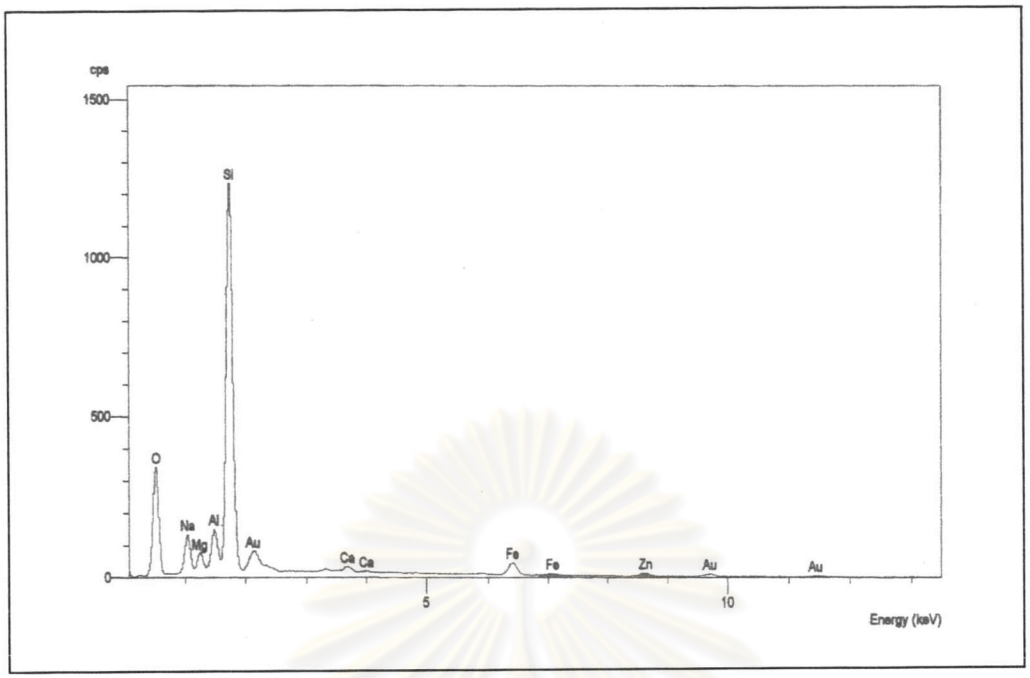

Fig.D-8 EDS spectra of dendritic crystal area (A) in GC#2 heat-treated at condition C

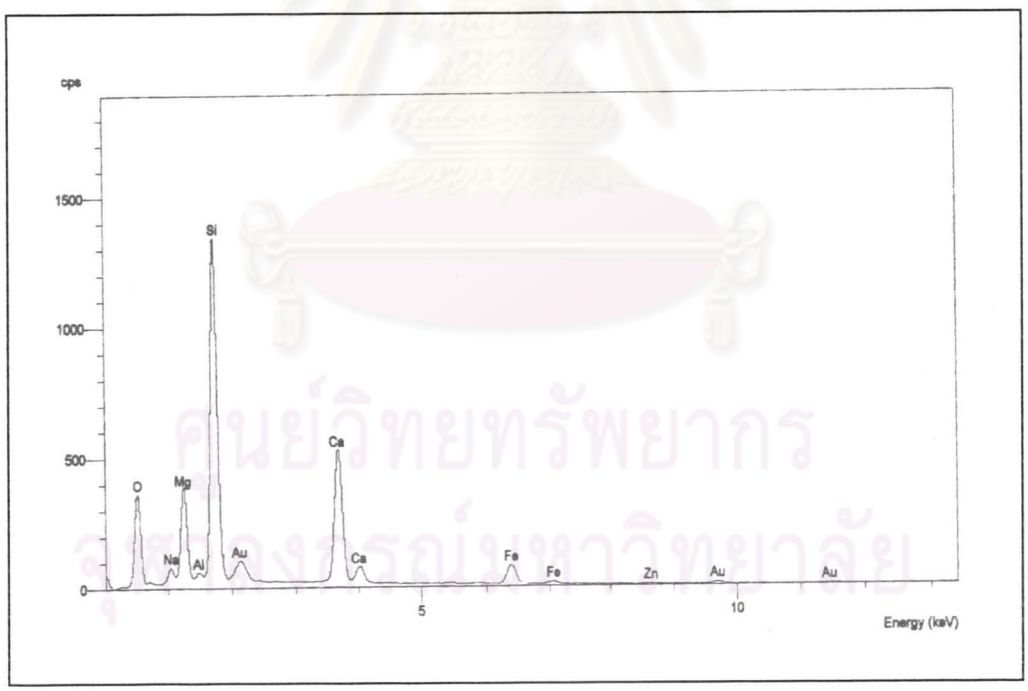

Fig.D-9 EDS spectra of glassy matrix area (B) in GC#2 heat-treated at condition C

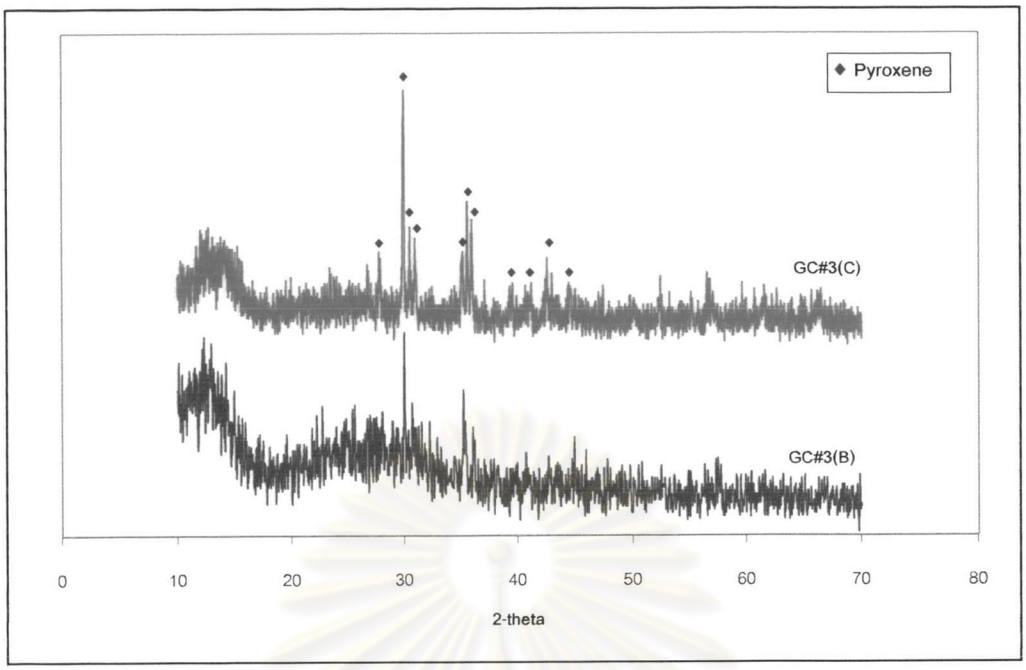

Fig.D-10 XRD patterns of GC#3 heat-treated at condition B and C

Fig.D-11 SEM micrographs (1500x) of pyroxene phase observed in GC#3 after heat-treatment at condition B (a) C (b)

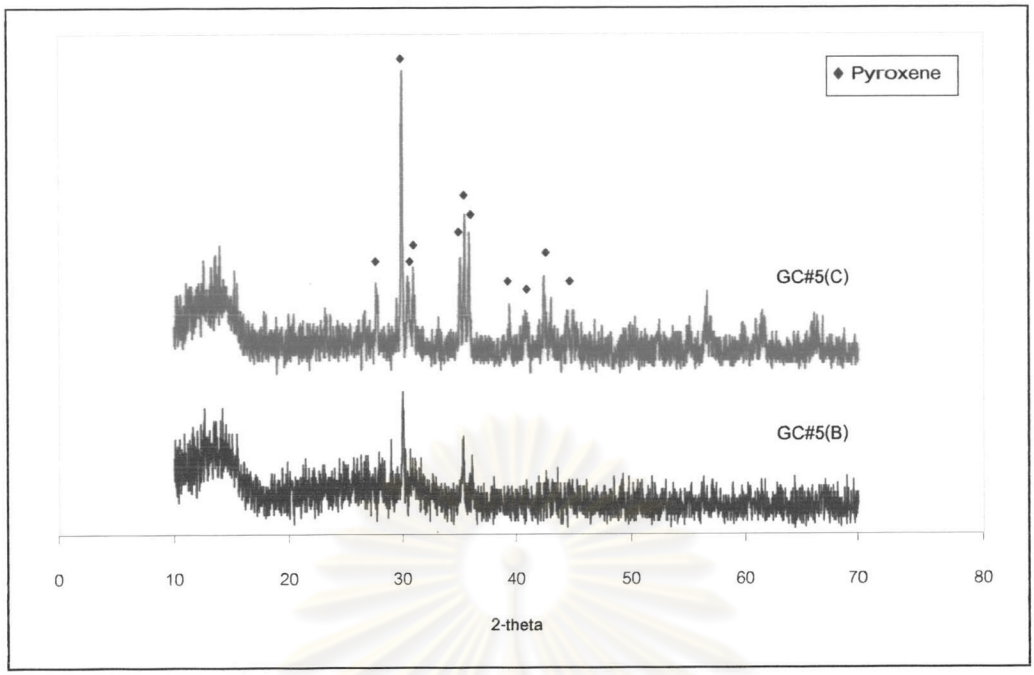

Fig.D-12 XRD patterns of GC#5 heat-treated at condition B and C

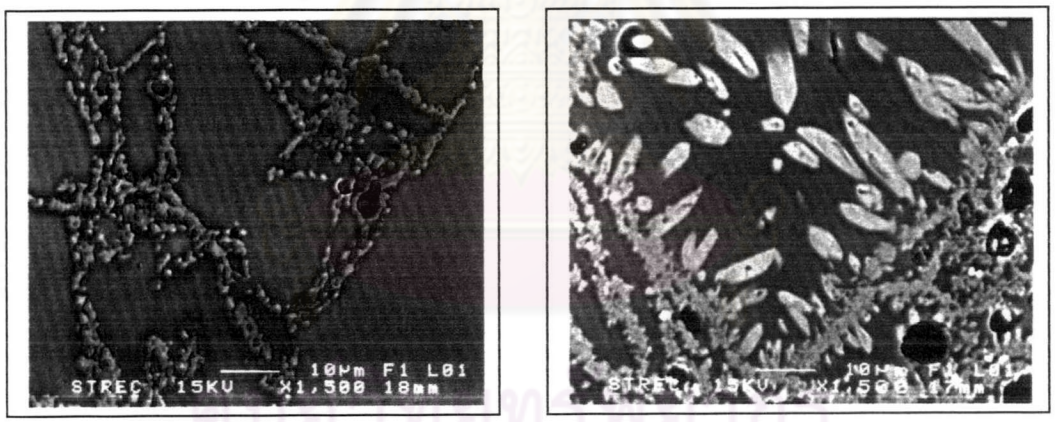

(a) (b)

Fig.D-13 SEM micrographs (1500x) of pyroxene phase observed in GC#5 after heat-treatment at condition B (a) C (b)

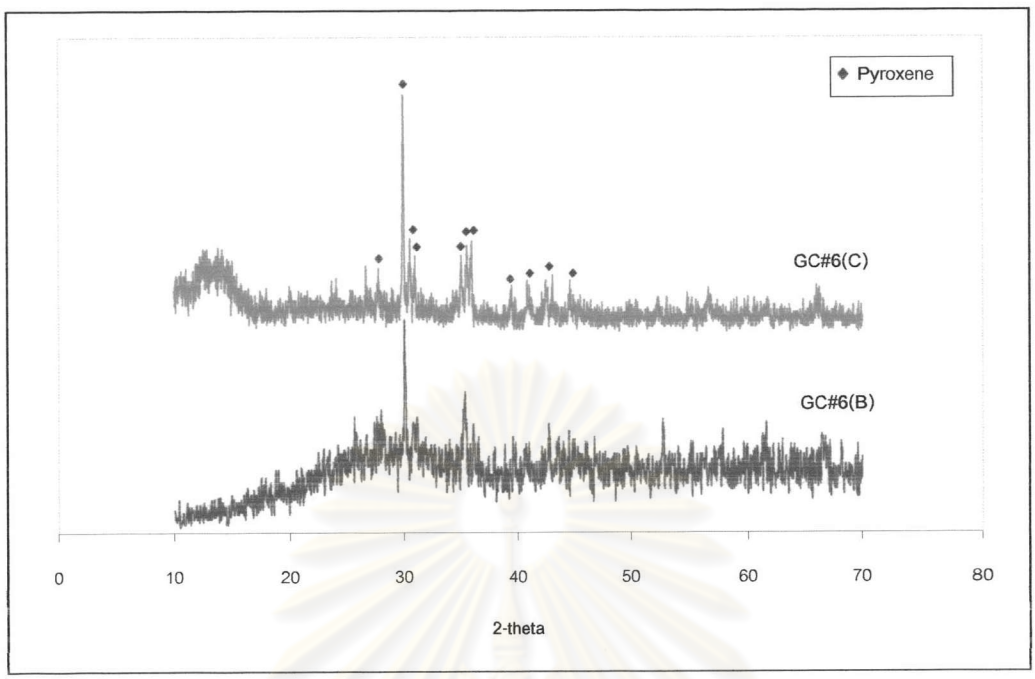

Fig.D-14 XRD patterns of GC#6 heat-treated at condition B and C

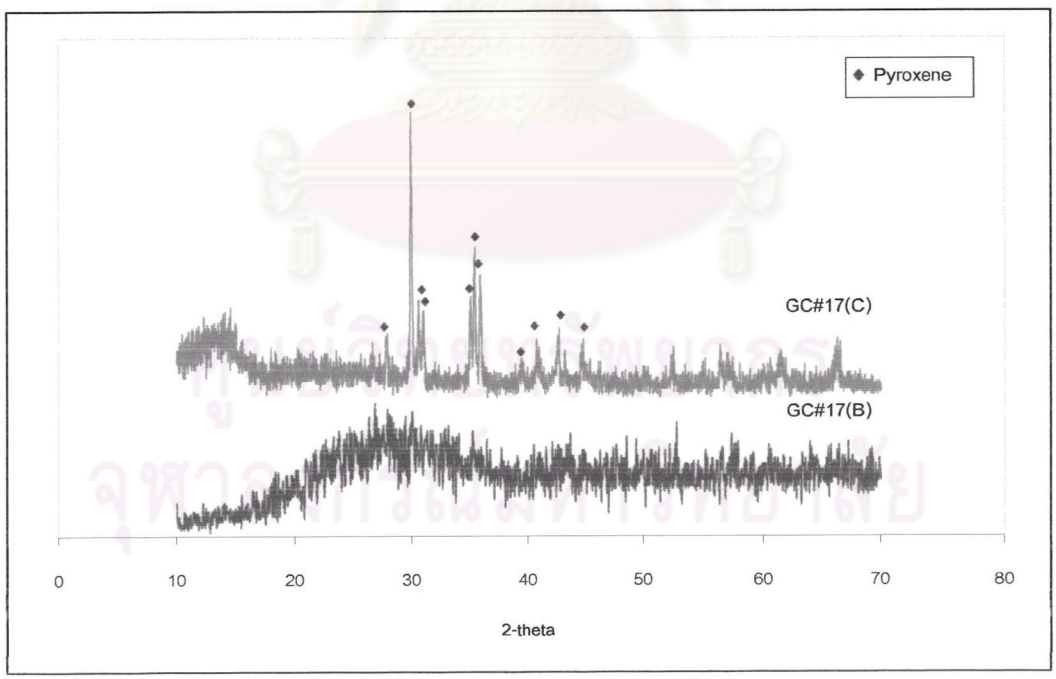

Fig.D-15 XRD patterns of GC#17 heat-treated at condition B and C

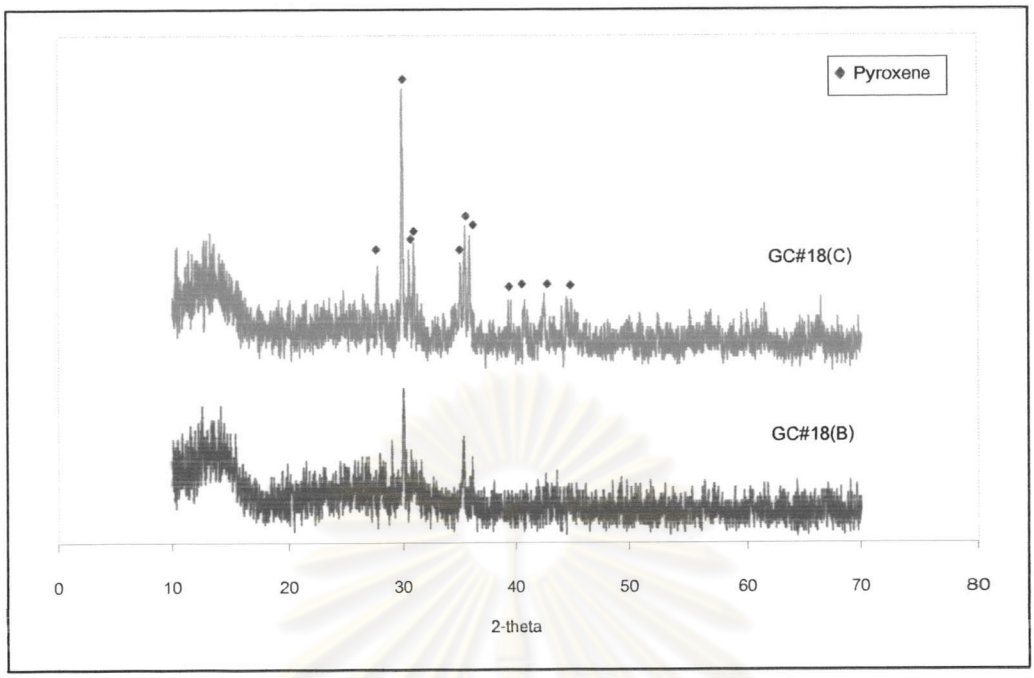

Fig.C-16 XRD patterns of GC#18 heat-treated at condition B and C

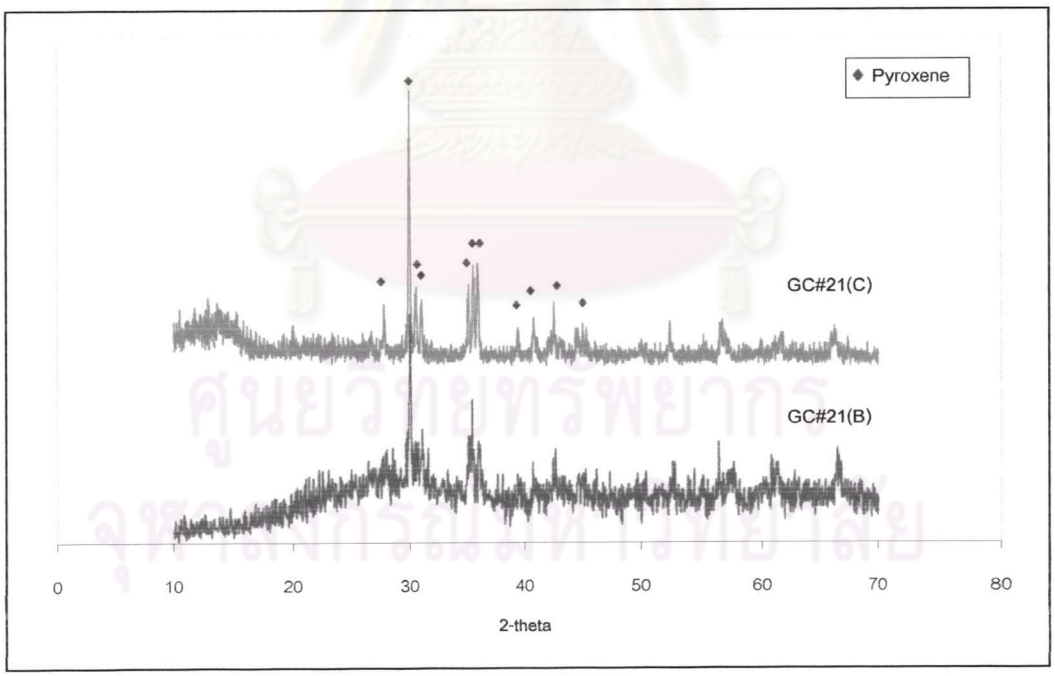

Fig.D-17 XRD patterns of GC#21 heat-treated at condition B and C

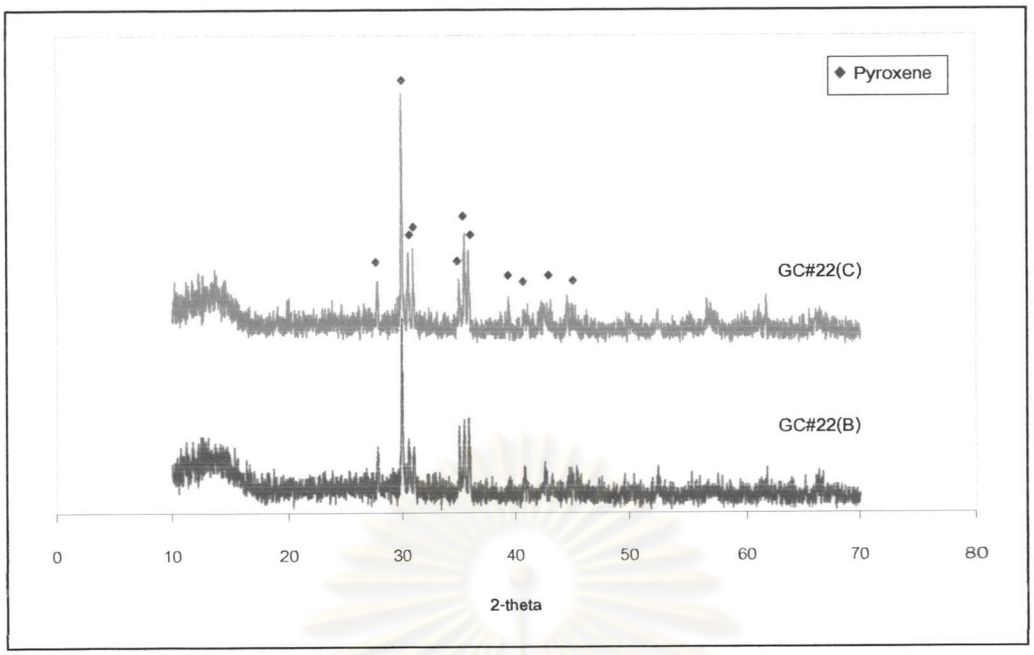

Fig.D-18 XRD patterns of GC#22 heat-treated at condition B and C

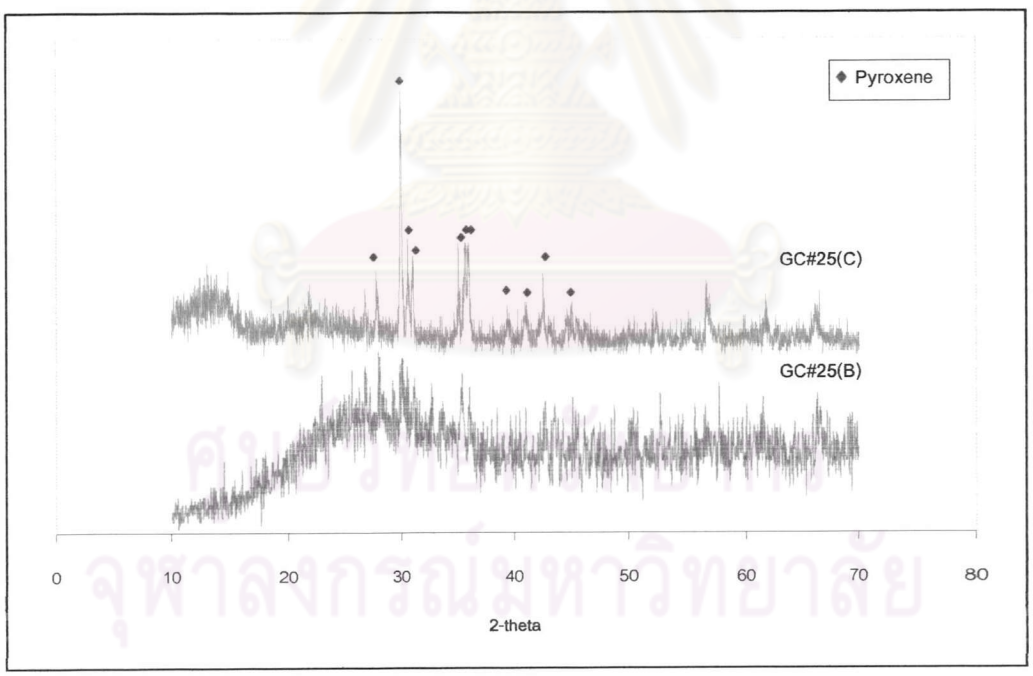

Fig.D-19 XRD patterns of GC#25 heat-treated at condition B and C

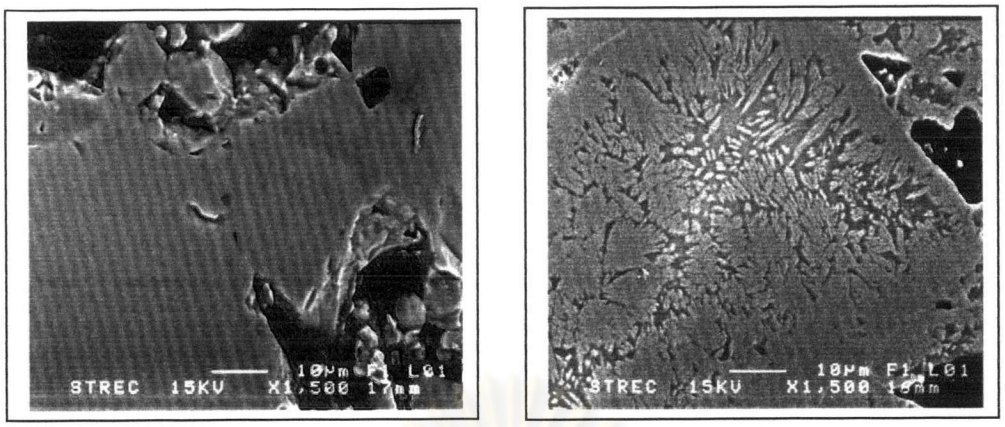

(a) (b)

Fig.D-20 SEM micrographs (1500x) of pyroxene phase observed in GC#25 after heat-treatment at condition B (a) C (b)

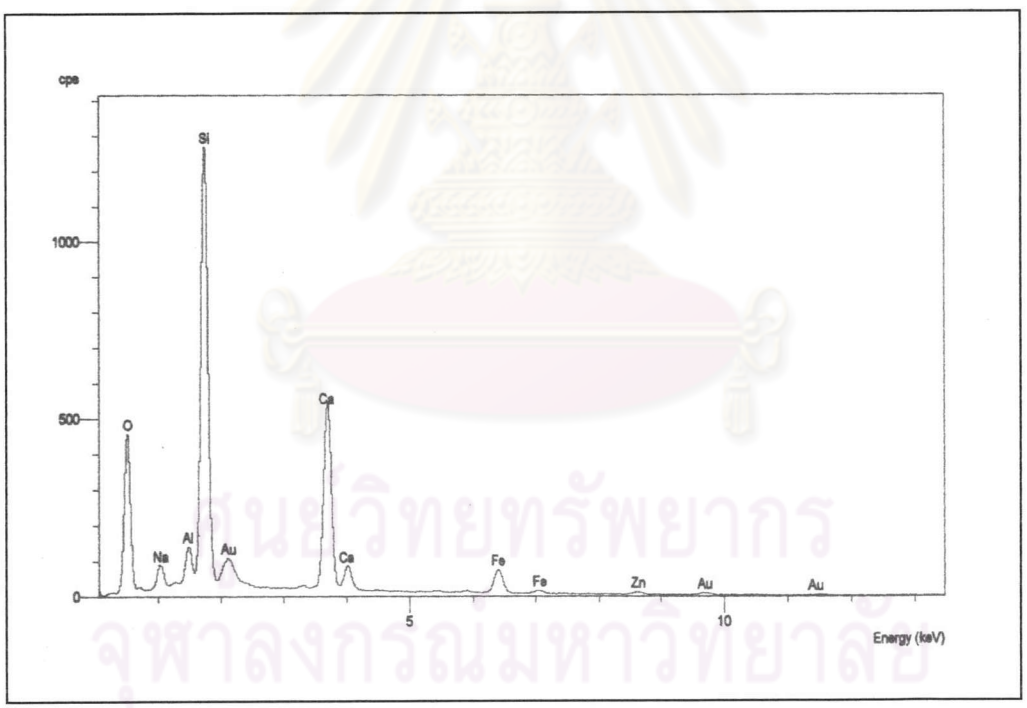

Fig.D-21 EDS spectra of area (A) in GC#13 heat-treated at condition C

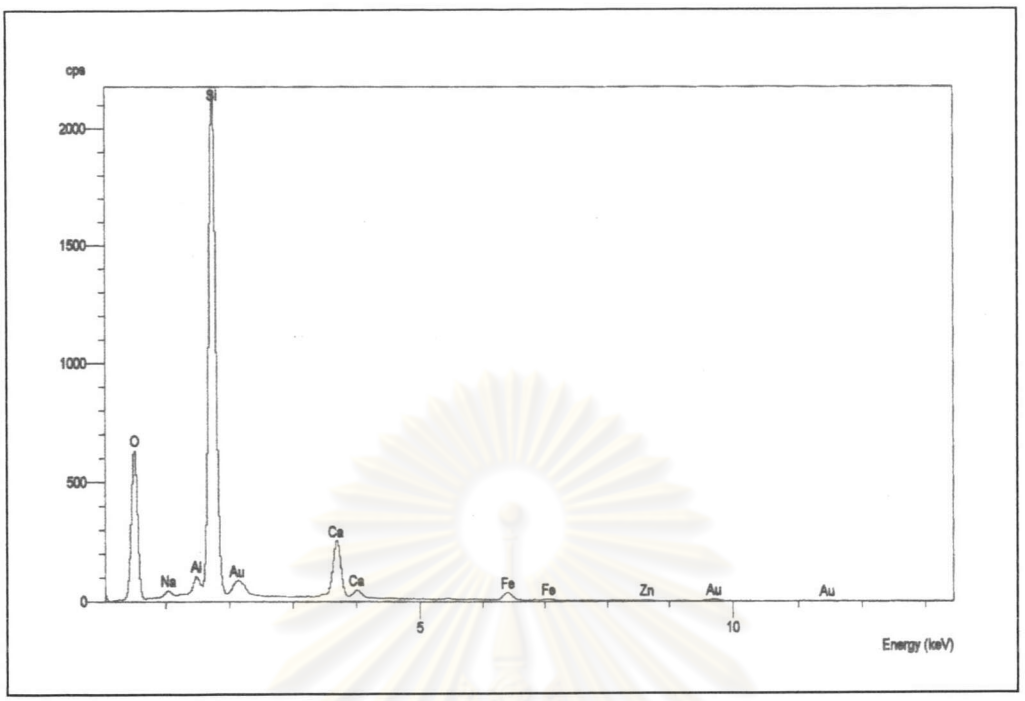

Fig.D-22 EDS spectra of area (B) in GC#13 heat-treated at condition C

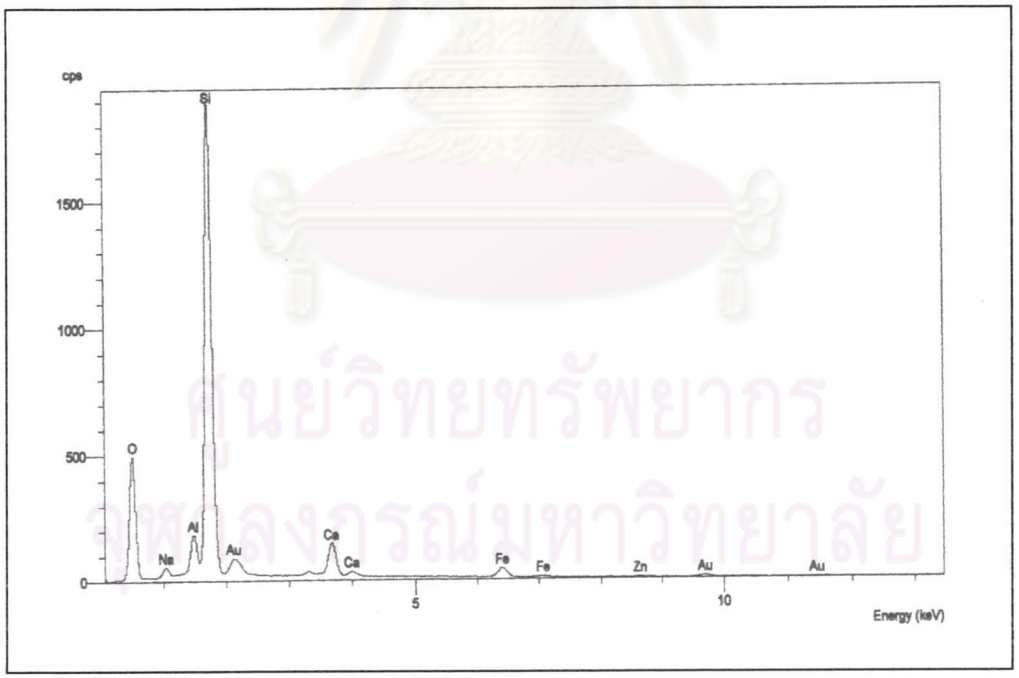

Fig.D-23 EDS spectra of area (C) in GC#13 heat-treated at condition C

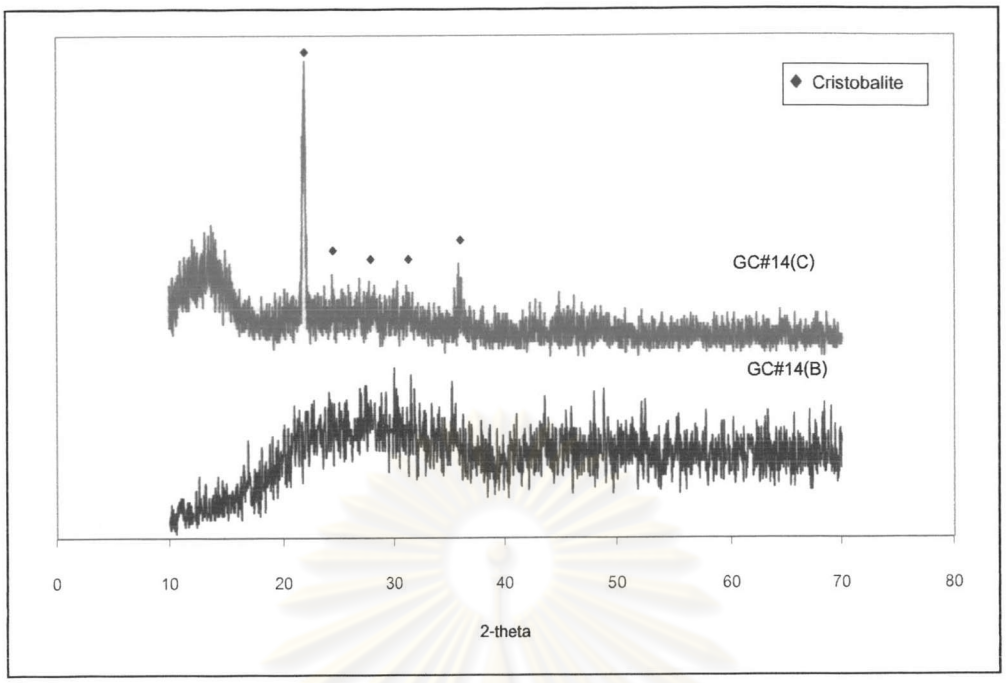

Fig.D-24 XRD patterns of GC#14 heat-treated at condition B and C

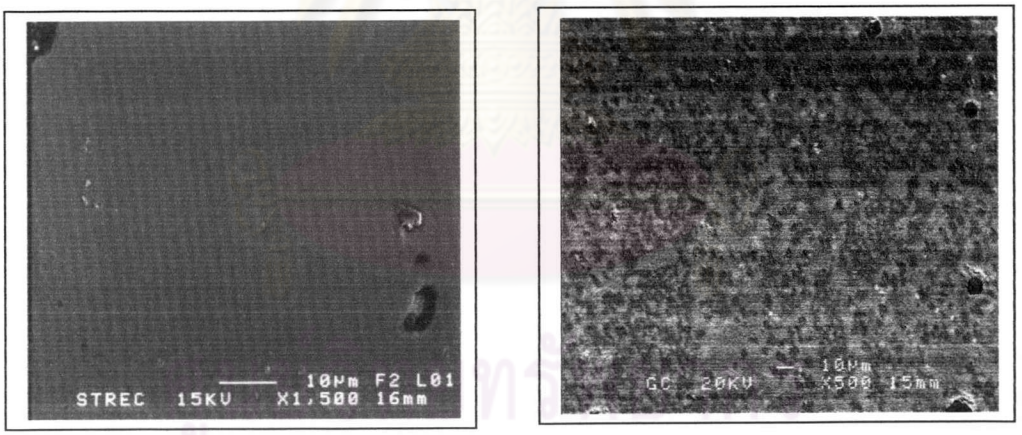

(a) (b)

Fig.D-25 SEM micrographs (1500x) of pyroxene phase observed in GC#14 after heat-treatment at condition B (a) C (b)

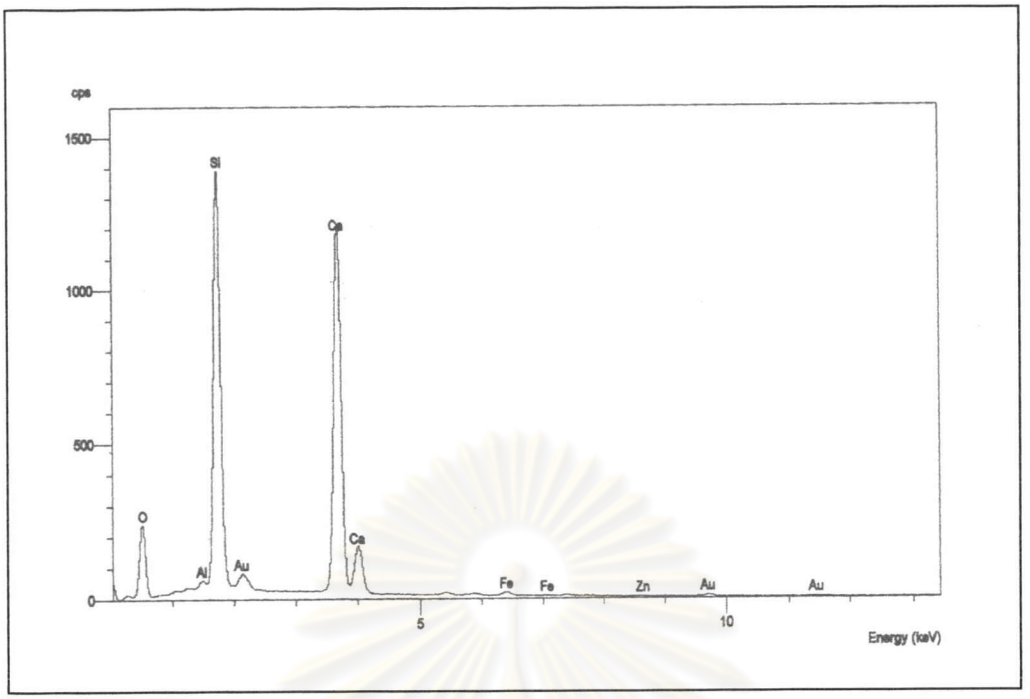

Fig.D-26 EDS spectra of acicular crystal area (A) in GC#4 heat-treated at condition C

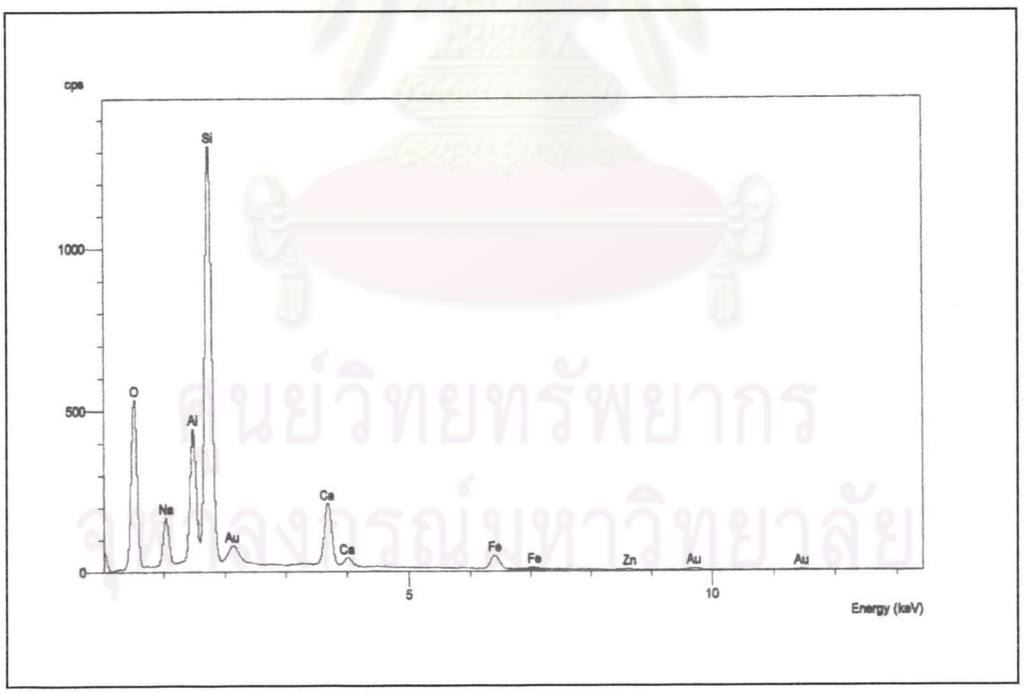

Fig.D-27 EDS spectra of black dendritic area (B) in GC#4 heat-treated at condition C

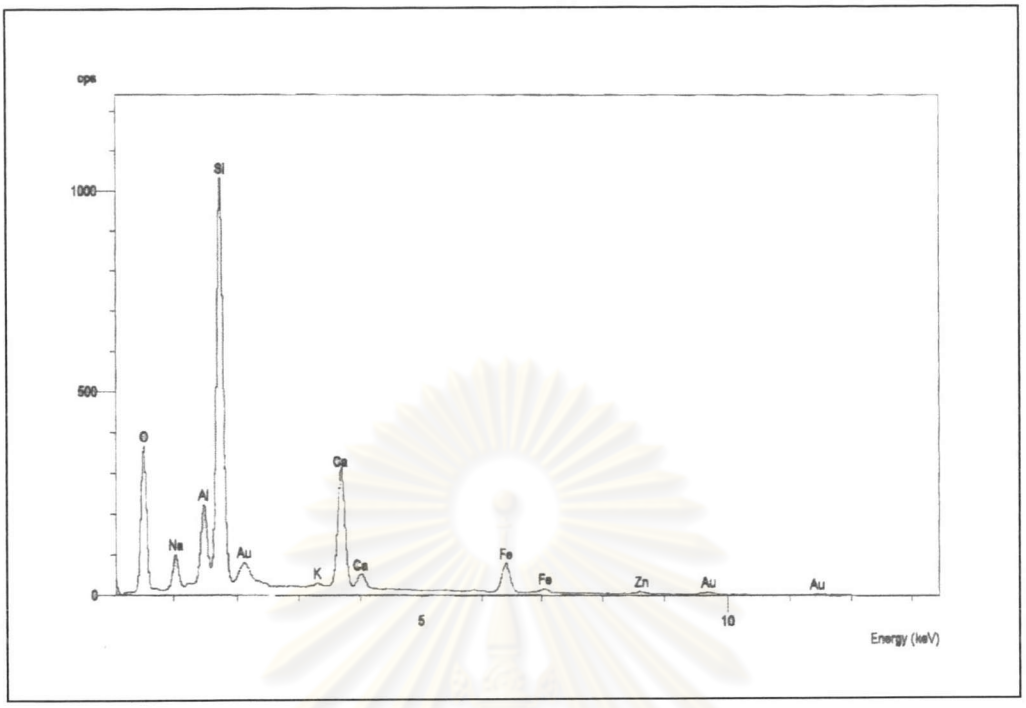

Fig.D-28 EDS spectra of glassy matrix area (C) in GC#4 heat-treated at condition C

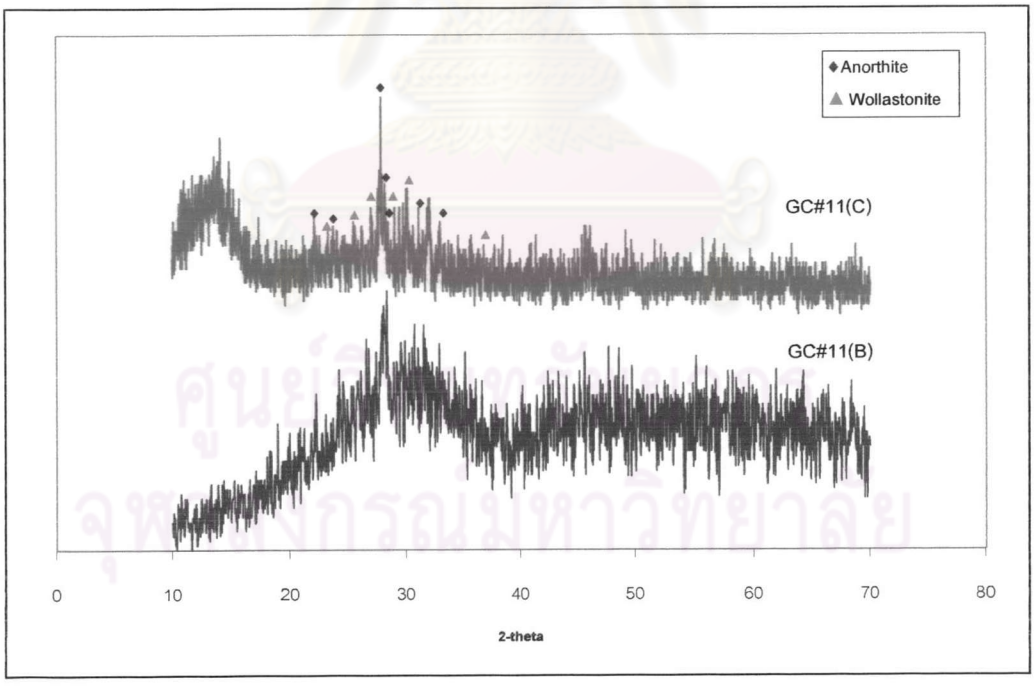

Fig.D-29 XRD patterns of GC#11 heat-treated at condition B and C

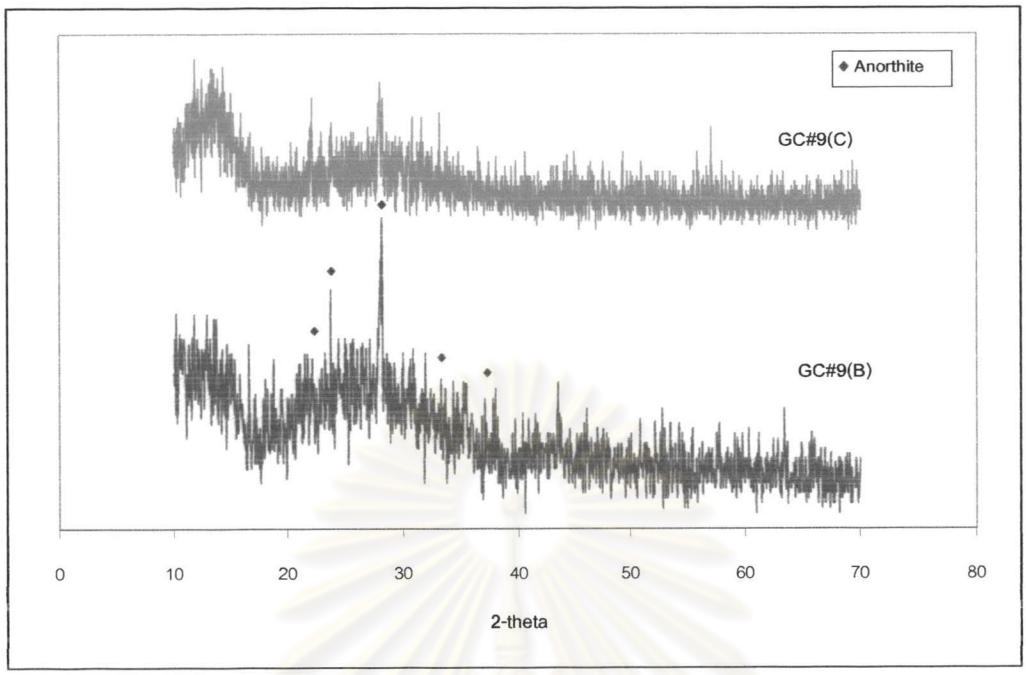

Fig.D-30 XRD patterns of GC#9 heat-treated at condition B and C

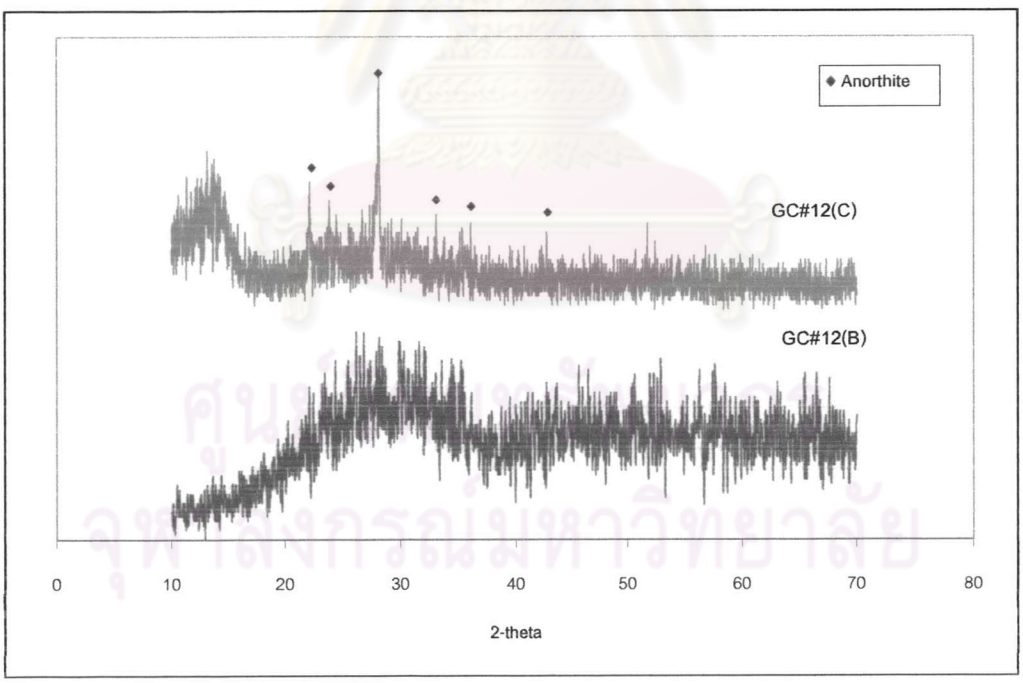

Fig.D-31 XRD patterns of GC#12 heat-treated at condition B and C

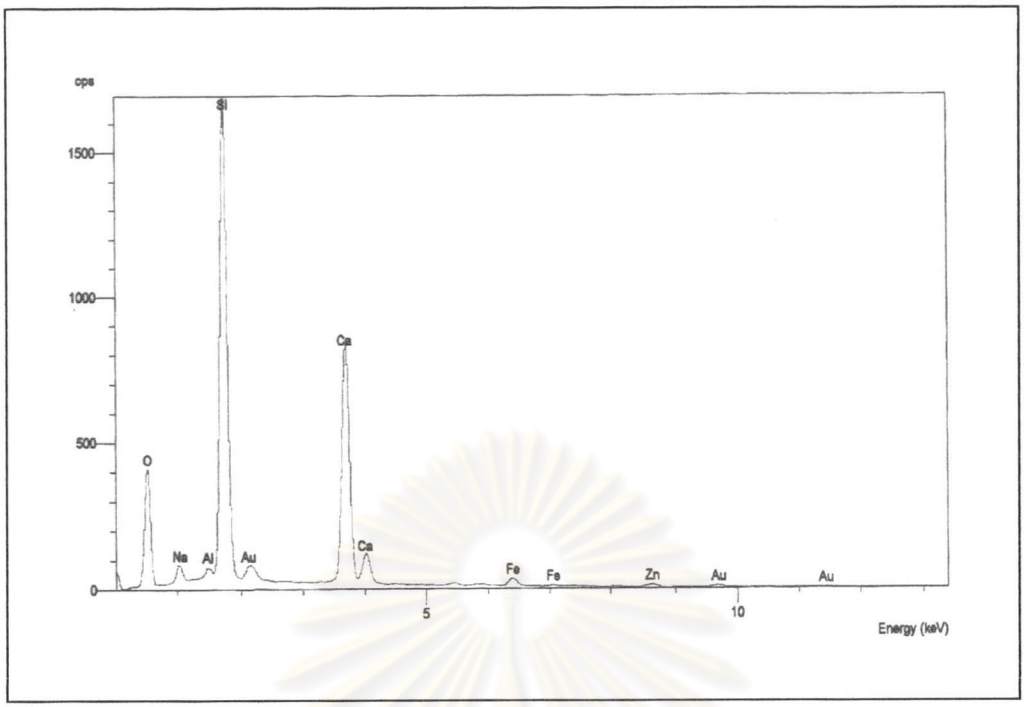

Fig.D-32 EDS spectra of acicular crystal area (A) in GC#19 heat-treated at condition C

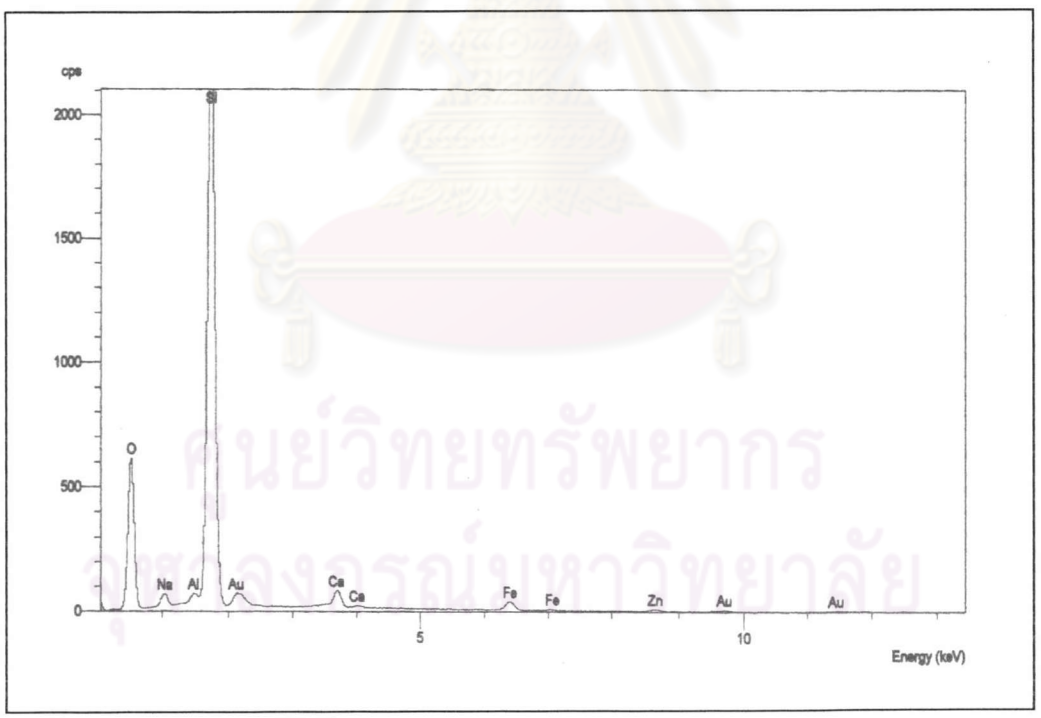

Fig.D-33 EDS spectra of dark dendritic crystal area (B) in GC#19 heat-treated at condition C

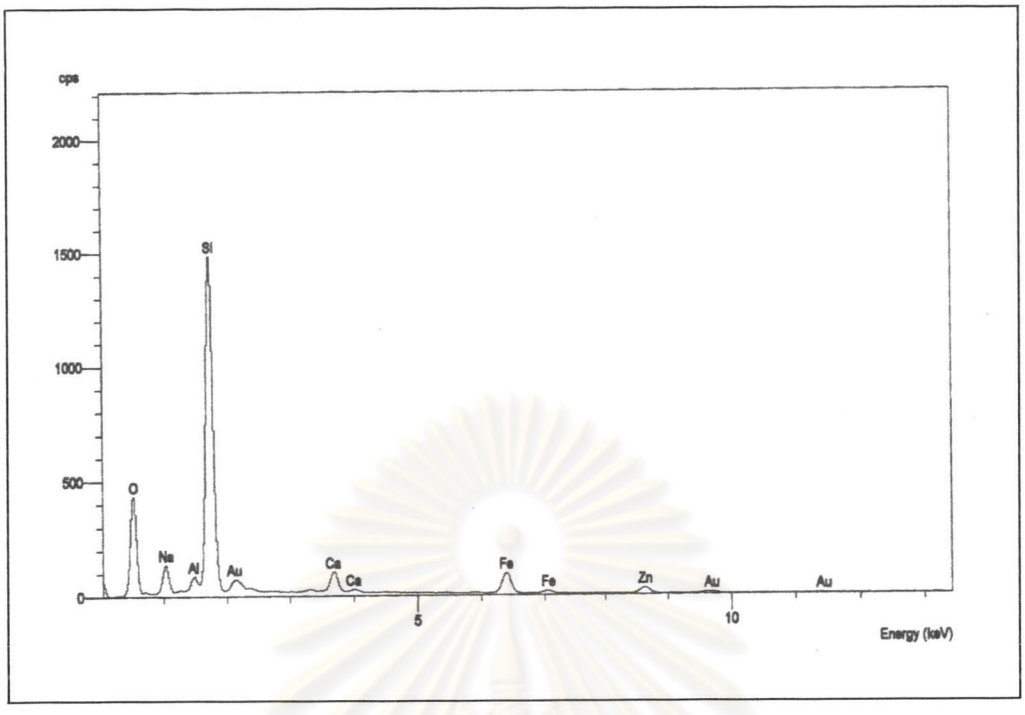

Fig.D-34 EDS spectra of glassy matrix area (C) in GC#19 heat-treated at condition C

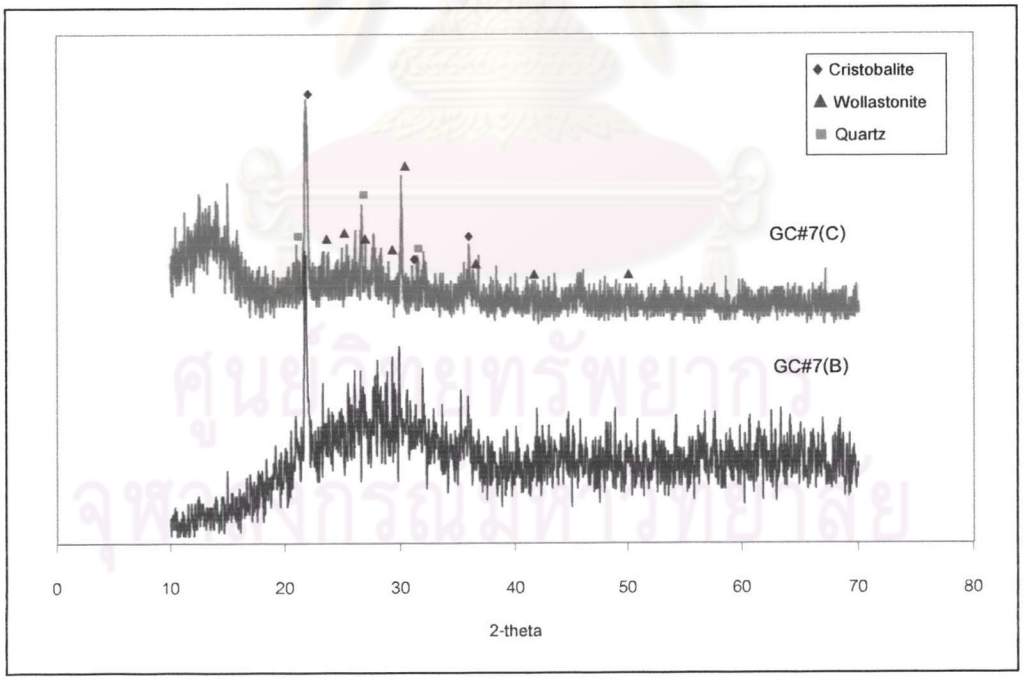

Fig.D-35 XRD patterns of GC#7 heat-treated at condition B and C

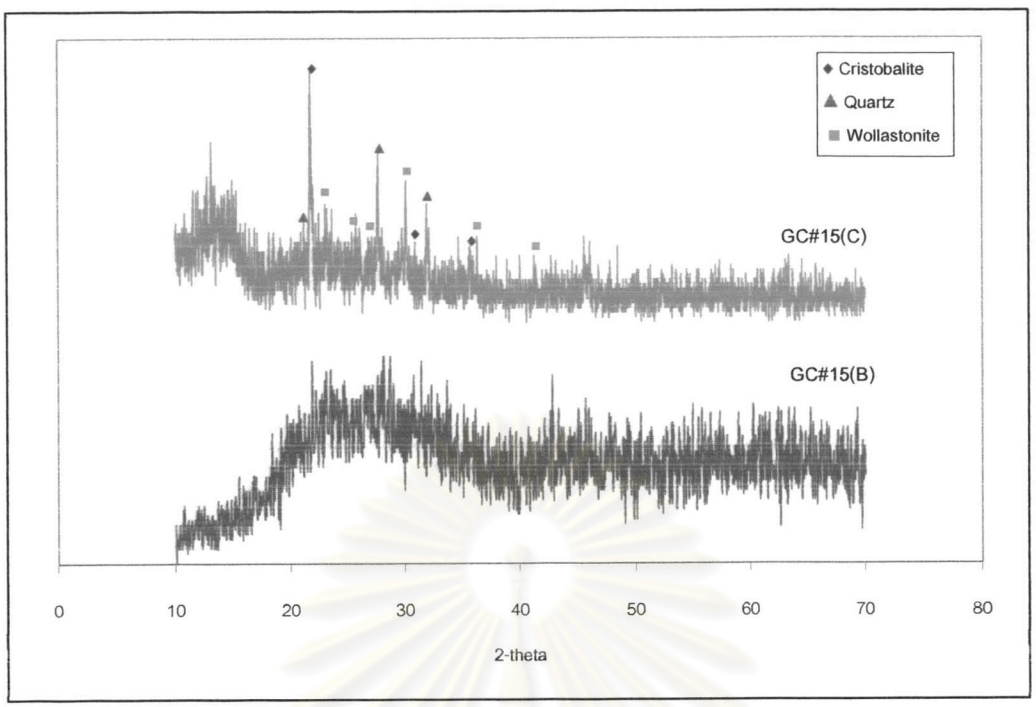

Fig.D-36 XRD patterns of GC#15 heat-treated at condition B and C

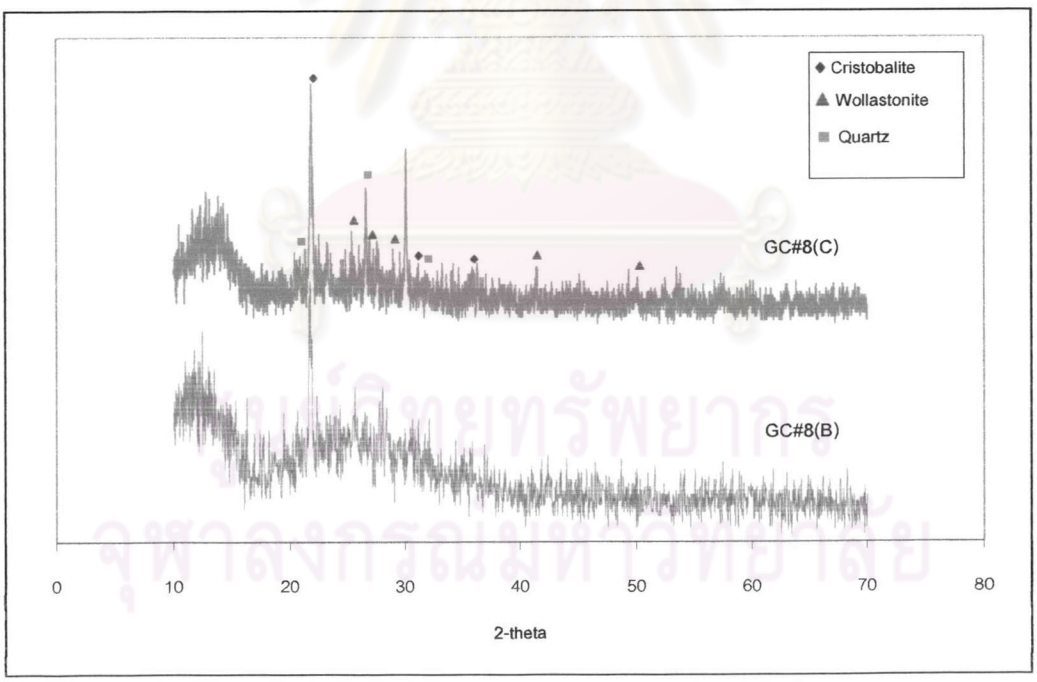

Fig.D-37 XRD patterns of GC#8 heat-treated at condition B and C

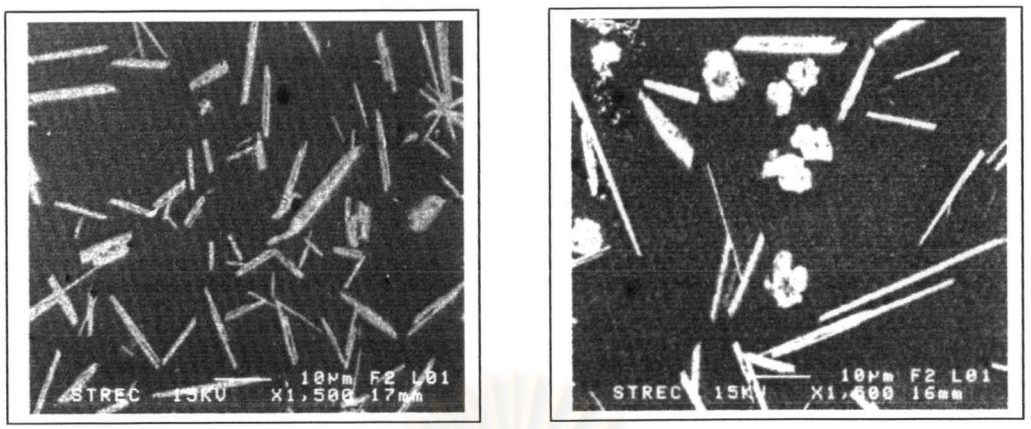

(a) (b)

Fig.D-38 SEM micrographs (1500x) of cristobalite, quartz and wollastonite-ferroan phase observed in GC#8 after heat-treatment at condition B (a) C (b)

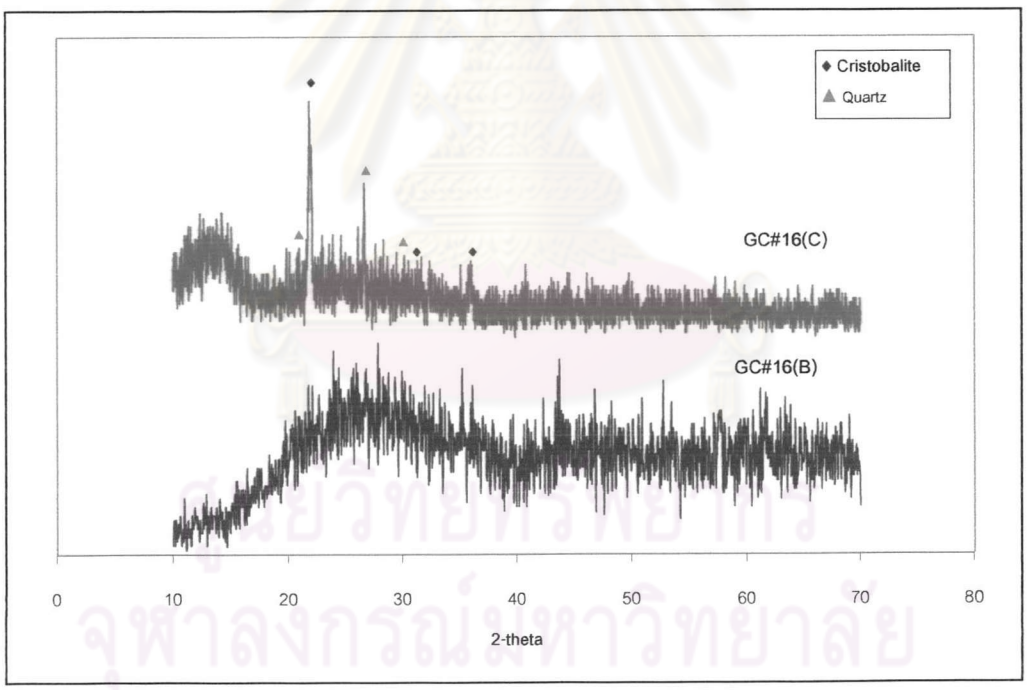

Fig.D-39 XRD patterns of GC#16 heat-treated at condition B and C

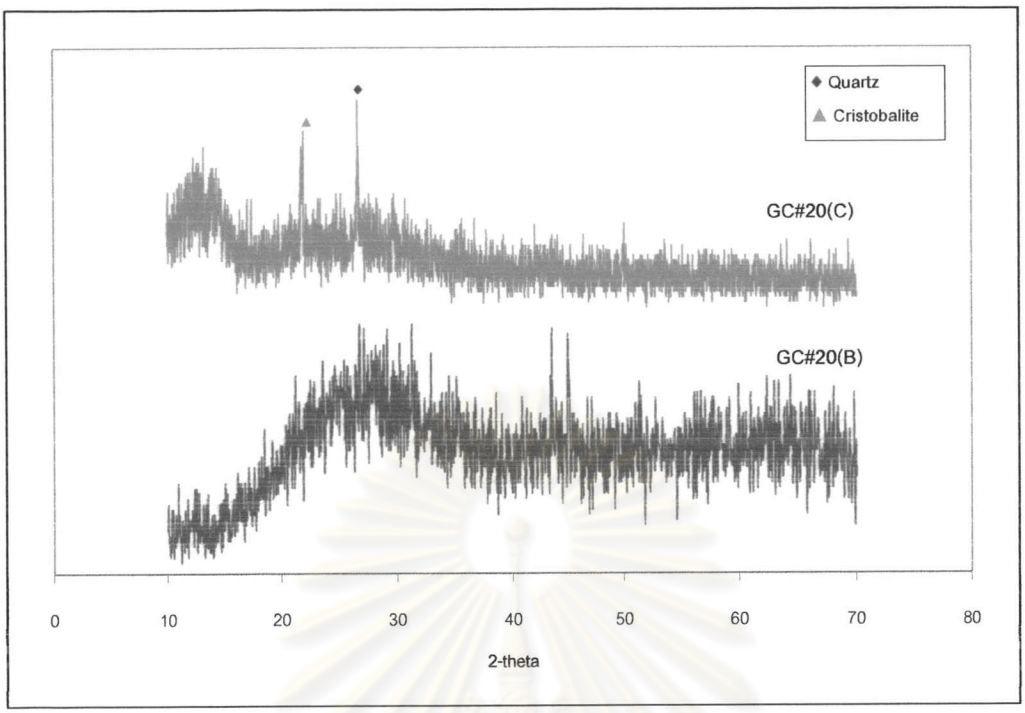

Fig.D-20 XRD patterns of GC#20 heat-treated at condition B and C

BIOGRAPHY

Miss Bussaraporn Patarachao was born in Chiang Rai on 30th September 1978. In 2001, after she had finished her Bachelor's Degree from Department of Physic, Faculty of Science, Chiang Mai University, she continued to study in Master's Degree in the field of Ceramic Technology at Chulalongkorn University. In 2003, she suspended her study to work at National Research Council (NRC) of Canada for one year, as she had received a Woman in Engineering and Science (WES) scholarship. The year after that she came back to Thailand and graduated in 2005.